Extracellular polymeric substances and algal bloom dynamics in sea ice

Anthony Jajeh[1], Kenneth M. Golden[2], Jody W. Deming[3], Jody R. Reimer[4]

Abstract

Algae living in the brine inclusions of polar sea ice produce a protective gelatinous coating of extracellular polymeric substances (EPS), which helps them survive in their harsh sea-ice habitat. One consequence of EPS production may be a reduction in nutrient availability, as EPS alters the ice microstructure, reducing permeability and the flux of nutrient-rich seawater into the ice. Here, we identify and analyze a novel biophysical feedback loop where algae modify their environment through EPS production, which then affects nutrient availability and subsequent algal growth. While mathematical models coupling nutrients and algae have been widely used to study bloom dynamics, here we introduce EPS as an additional variable to investigate this feedback and its role in microbial strategies for living in such an extreme environment as sea ice. Analysis of both transient and asymptotic dynamics suggests that EPS-mediated feedbacks suppress algal biomass in both the short and long term. Quasi-steady-state analysis of our model reveals a transcritical bifurcation governed by nutrient fluxes, indicating a threshold beyond which the system transitions from a barren state to one supporting microbial life. We also identify a Hopf bifurcation, which suggests that EPS-mediated negative feedbacks can give rise to sustained oscillations in nutrient and algal biomass levels. These results highlight how the tight coupling between EPS production, nutrient transport, and algal dynamics fundamentally shapes both sea-ice primary productivity and permeability.

1 Introduction

Polar sea ice hosts a dynamic community of microscopic inhabitants within its porous microstructure (Thomas and Dieckmann (2010)), which forms as seawater freezes. While much of the salt in seawater is expelled during freezing, some remains trapped within the ice, concentrated in liquid brine, creating a complex network of brine-filled inclusions (Lake and Lewis (1970); Petrich and Eicken (2009); Zong (2022)). The volume fraction, geometry, and connectivity of these inclusions depend strongly on temperature, crystalline structure, and conditions under which the ice was formed (Petrich and Eicken (2009); Thomas and Dieckmann (2010)). Ice algae dominate these brine inclusions in spring, when light becomes sufficient to support algal blooms in the ice (Stoecker et al. (2000)). Ice algae contribute significantly (up to 26% (Gradinger (2009))) to total primary production in the polar regions (Arrigo et al. (2008)). Due to their early availability in spring and lipid-rich composition (Gradinger (2009)), ice algae are foundational to the polar marine food web, supporting grazers such as zooplankton, which in turn support higher trophic levels, including fish, seabirds, whales, seals, and polar bears (Stoecker et al. (2000)). For example, a high percentage of a polar bear's diet (on average about 86% (Brown et al. (2018))) can be traced back to sea-ice algae.

Ice algae must endure extreme environmental conditions within the ice, including low temperatures, high salinity, and low light availability for much of the year. Many sea-ice microbes, including ice algae, have adapted by producing a cryoprotective gelatinous coating of extracellular polymeric substances (EPS), a complex mix of polysaccharides, proteins, and other components (Ewert and Deming (2013); Krembs et al. (2011)). In addition to acting as a buffer between the microbes and

[1]University of Utah, Department of Mathematics, Salt Lake City, UT, USA,jajeh@math.utah.edu ORCID: 0009-0009-5546-5781
[2]University of Utah, Department of Mathematics and adjunct in Department of Biomedical Engineering, Salt Lake City, UT, USA. ken.golden@utah.edu, ORCID: 0000-0002-1688-183X
[3]University of Washington, School of Oceanography, Seattle, WA, USA. jdeming@uw.edu, ORCID: 0000-0002-0310-1101
[4]University of Utah, Department of Mathematics and School of Biological Sciences, Salt Lake City, UT, USA. jody.reimer@utah.edu, ORCID: 0000-0001-7742-2728

their environment, EPS alters the physical properties of the surrounding ice (Krembs et al. (2011); Roukaerts et al. (2021)). The presence of EPS, whether coating cells or released into their surroundings, changes the geometry of the pores and may impede fluid flow through clogging effects, altering the flux of nutrients available to the microbial community (Krembs et al. (2011); Steffen et al. (2018)). Reduced nutrient fluxes (in particular, nitrogen) limit algal growth (Gradinger (2009)), and because algae are the largest producers of EPS, this is hypothesized to subsequently decrease EPS production rates. This suggests a complex EPS-mediated biophysical feedback, with implications for both sea-ice physics and ecosystem dynamics. For example, can a bloom be so successful with so much EPS produced that the clogging, which can restrict vital nutrient fluxes, provides a check or negative feedback on the growth, thus regulating the bloom?

In this paper, we take the first step toward understanding the biophysical feedback dynamics mediated by EPS. We begin with a canonical algal bloom model and extend it to include EPS as a new variable (Section 2). This extended model is a coupled set of ordinary differential equations that describes the interactions among nutrients, algae, and EPS. While we do not explicitly model sea ice microstructure, the effect of EPS on ice permeability is included through nonlinear terms that capture its impact on nutrient fluxes. In Section 2.1, we analyze the most general form of the model to understand its key features of asymptotic behavior. In Section 2.2, we explore model sensitivity to the timescales over which EPS accumulate and decay, as these processes are difficult to measure empirically and thus poorly constrained in our model. We analyze three model regimes corresponding to three timescale assumptions: EPS dynamics are much slower than algal and nutrient dynamics (Regime 1, Section 2.2.1); EPS dynamics are fast, responding instantaneously to changes in algal biomass (Regime 2, Section 2.2.2); and EPS dynamics occur over similar timescales to those of algae and nutrients (Regime 3, Section 2.2.3). We conduct a bifurcation and stability analysis of our model under each of these assumptions. Comparison between regimes (Section 2.3) reveals a persistent transcritical bifurcation that depends on nutrient flux terms, and a Hopf bifurcation that is only possible if EPS dynamics occur over similar timescales to those of algae and nutrients (Regime 3). This Hopf bifurcation suggests that strong EPS-mediated negative feedbacks may induce periodic algal growth and, fascinatingly, concurrent periodic changes in ice permeability. Finally, in Section 2.4, we investigate the system's transient bloom dynamics through numerical simulations. These simulations, in showing an inverse relationship between EPS accumulation and peak bloom intensity, suggest that the negative EPS-mediated biophysical feedbacks that are the focus of this paper do indeed reduce peak algal concentrations. Our model thus begins to address the questions raised above concerning the role of EPS in regulating bloom dynamics.

2 Model formulation

We begin with a classic model of nutrient-driven phytoplankton blooms (Huppert et al. (2002)), which captures the main processes and functional forms commonly found in sea ice biogeochemical models (Lannuzel et al. (2020); Miller et al. (2015); Roukaerts et al. (2021); Tedesco and Vichi (2014)).

$$\frac{dN}{dt} = \alpha - \frac{\nu N A}{\gamma + N} - \beta N$$
$$\frac{dA}{dt} = \xi \frac{\nu N A}{\gamma + N} - \delta A$$

Typically, this model describes the dynamics of a limiting nutrient N and phytoplankton P; however, since ice algae are our primary producers of interest, we have changed the notation from P to A. We have chosen nitrogen as the nutrient of interest, as nitrogen limitation is considered to inhibit ice algal blooms (Kim et al. (2020)). Field measurements are often technically of particulate nitrogen, which refers to nitrogen-containing compounds (both organic and inorganic) suspended in meltwater from cores (Krembs et al. (2011)). Nutrient fluxes are described by input (α) and loss (β) rates, assuming nutrients enter the brine inclusions from the ocean below, facilitated by convective processes within the ice (Petrich and Eicken (2009)). Nutrient loss by algae is described by the Monod term in both equations, where ν is the maximum uptake rate, γ is the half-saturation constant, and ξ is the rate of algal growth corresponding to nutrient uptake. Algae are lost at a rate δ due to death or loss from the ice. All parameter values are assumed to be positive. Note that this model assumes constant, optimal light for photosynthesis, and an unchanging ice environment corresponding to stable temperatures.

We now adapt this model to study EPS-mediated biophysical feedbacks. We add E, a state variable describing the concentration of EPS in the system, often in units of milligrams of Xanthan

Gum equivalent per liter (mg XG/L) (Krembs et al. (2002)). We assume that the EPS accumulation rate (ρ) is proportional to the amount of algae present, and that it decays at a constant rate (η). As EPS accumulates, it clogs the brine inclusions, reducing nutrient fluxes (Krembs et al. (2011)). To capture this process, we replace the parameters α and β in the above equations with EPS-dependent functions, $\alpha(E)$ and $\beta(E)$. In general, these functions are assumed to be nonnegative and monotonically decaying with E. The resulting model of coupled nutrient, algae, and EPS dynamics is

$$\begin{aligned} \frac{dN}{dt} &= \alpha(E) - \frac{\nu N A}{\gamma + N} - \beta(E) N \\ \frac{dA}{dt} &= \xi \frac{\nu N A}{\gamma + N} - \delta A \\ \frac{dE}{dt} &= \rho A - \eta E \end{aligned} \tag{1}$$

Table 1 describes the units of each model component and the values of model parameters, where available, from the literature.

2.1 A nutrient-driven transcritical bifurcation

Empirical estimates of the best form for the nutrient flux functions, $\alpha(E)$ and $\beta(E)$, do not exist, so we first conduct a preliminary analysis of model (1) without explicitly specifying functional forms. Setting $\frac{dN}{dt} = \frac{dA}{dt} = \frac{dE}{dt} = 0$, we find two steady-state solutions for (N^*, A^*, E^*):

$$\begin{aligned} s_0 &\coloneqq \left(\frac{\alpha(0)}{\beta(0)}, 0, 0 \right) \\ s_1 &\coloneqq \left(\frac{-\delta\gamma}{-\xi\nu + \delta}, \frac{\xi\beta(E)}{\delta(\delta - \xi\nu)} \left(\gamma\delta + \frac{\alpha(E)}{\beta(E)}(\delta - \xi - \nu) \right), \frac{\rho A^*}{\eta} \right) \end{aligned}$$

Observe that s_0 is a trivial steady state, characterized by the absence of both algae and EPS, while s_1 is a nontrivial steady state in which algae and EPS persist. To assess the stability of s_0, we analyze the Jacobian of (1) evaluated at this steady state (see S1), which yields the following eigenvalues:

$$\lambda_1 = -\eta, \quad \lambda_2 = -\beta(0), \quad \lambda_3 = \frac{\xi\nu\alpha(0) - \beta(0)\,\gamma\delta - \alpha(0)\,\delta}{\gamma\beta(0) + \alpha(0)}$$

Because all model parameters and α and β are positive, λ_1 and λ_2 are negative, and the sign of λ_3 depends on the sign of its numerator. Rearranging, we see that if $\alpha(0)/\beta(0) < \gamma\delta/(\xi\nu - \delta)$, then $\lambda_3 < 0$ and s_0 is a stable node. So if the ratio of physical nutrient input to loss in the absence of EPS, $\alpha(0)/\beta(0)$, is sufficiently small, the system will eventually approach an algae- and EPS-free state. However, if $\alpha(0)/\beta(0)$ is sufficiently large, then $\lambda_3 > 0$ and s_0 is unstable. This scenario is a transcritical bifurcation in the ratio of nutrient input to loss in an EPS-free system, $\alpha(0)/\beta(0)$. This behavior provides a key ecological insight: algae persist only when the advective nutrient inflow is sufficiently large relative to the physical nutrient outflow, replenishing the nutrients needed to sustain the algal population. We will see this insight reflected in several places in the analysis that follows.

The nontrivial equilibrium s_1 is only defined if all state variables are nonnegative, that is, if $\frac{\alpha(E)}{\beta(E)} \geq \frac{\gamma\delta}{\nu\xi - \delta}$, with $\delta < \xi\nu$. We cannot further analyze the existence and stability of s_1 without specifying functional forms for $\alpha(E)$ and $\beta(E)$. Here we choose to use a negative exponential function, which captures the hypothesis that higher EPS reduces nutrient fluxes. We define $\alpha(E) = \phi \exp(\frac{-E}{\mu})$ and $\beta(E) = \psi \exp(-\frac{E}{\mu})$, where ϕ and ψ represent the nutrient input and loss rates in the absence of EPS, respectively, and μ is the strength of EPS limitation. This approach results in the fully specified model

$$\begin{aligned} \frac{dN}{dt} &= \phi e^{-\frac{E}{\mu}} - \frac{\nu N}{\gamma + N} A - \psi e^{-\frac{E}{\mu}} N \\ \frac{dA}{dt} &= \xi \frac{\nu A N}{\gamma + N} - \delta A \\ \frac{dE}{dt} &= \rho A - \eta E \end{aligned} \tag{2}$$

Symbol	Biological Description	Value	Range	Units	Source
N	Average concentration of particulate nitrogen	N/A	0.1–0.2	mg N/L	(Krembs et al. (2011)) Supp. Table S2
A	Mean chl-a in bottom 10 cm of sea ice	N/A	0.03–0.06	mg/L	(Krembs et al. (2011)) Supp. Table S2
E	EPS concentration	N/A	0.8–7.7	mg XG/L	(Krembs et al. (2002))
N_0	Initial condition for nutrient	0.2	-	mg N/L	Prescribed
A_0	Initial condition for algae	0.0002	-	mg A/L	Prescribed
E_0	Initial condition for EPS	0.002	-	mg XG/L	Prescribed
ϕ	Inflow rate of nutrients	0.01	-	mg N/(L day)	Prescribed
ψ	Outflow rate of nutrients	0.01	-	1/day	Prescribed
ν	Nutrient uptake rate by bottom ice algae	0.2	0.24	mg N/(mg chl-a day)	(Kim et al. (2020))
ρ	Production rate of EPS	.75	0.1–1	mg XG/(mg chl-a L day)	(Krembs et al. (2002))
δ	Mortality rate of ice algae	0.007	0.007	1/day	(Hunke et al. (2024))
η	Bacterial degradation of polysaccharides	0.03	0.03	1/day	(Hunke et al. (2024))
γ	Half-saturation constant of ice algae nitrogen uptake rate	0.01	0.01	mg N/L	(Hunke et al. (2024))
ξ	Algal chl-a to nitrogen conversion ratio	0.2	0.2	mg chl-a/mg N	(Hunke et al. (2024))
μ	Strength of EPS feedback	0.001	-	mg XG/L	Prescribed
σ	Scaling of how EPS tracks algae in Regime 2	0.05	-	-	Prescribed

Table 1: State variables and parameter values used throughout this work. Rows for the state variables N, A, and E describe their observed average concentrations in spring sea ice for comparison with our model outputs. The Value column contains the parameter values chosen as the defaults for all figures produced in the text unless noted otherwise. The Range column contains the parameter ranges documented in the literature described under Source.

2.2 Model analysis under different timescale assumptions

Quantifying EPS in sea ice is difficult. While EPS can be detected and visualized in sea ice via Alcian Blue staining, the existing methods for quantitative measurements require melting the ice to extract the EPS, making in situ serial measurements currently impossible (Miller et al. (2015)). Because of this, little is known about how rapidly EPS accumulate or decay within sea ice. We explore three possible temporal regimes by modifying and analyzing (2) accordingly.

2.2.1 Regime 1: EPS dynamics are much slower than algal and nutrient dynamics

We start by nondimensionalizing (2) (see Appendix 8) with this temporal scaling in mind, which results in two fast equations and one slow one,

$$\textbf{Fast} \begin{cases} \epsilon \frac{dN}{d\tau} = ae^{-E} - \frac{cAN}{N+1} - bNe^{-E} \\ \epsilon \frac{dA}{d\tau} = \frac{fNA}{N+1} - A \end{cases} \tag{3a}$$

$$\textbf{Slow} \begin{cases} \frac{dE}{d\tau} = dA - E \end{cases} \tag{3b}$$

We now perform a quasi-steady-state analysis of our system. To analyze the fast set of equations, we scale time by ϵ, that is, $\tau' = \frac{\tau}{\epsilon}$. Then (3) becomes:

$$\frac{dN}{d\tau'} = ae^{-E} - \frac{cAN}{N+1} - bNe^{-E} \tag{4a}$$

$$\frac{dA}{d\tau'} = \frac{fNA}{N+1} - A \tag{4b}$$

$$\frac{dE}{d\tau'} = \epsilon(dA - E) \tag{4c}$$

We now let $\epsilon \to 0$. In the dimensional model, this is equivalent to $\epsilon = \eta/\delta \to 0$, which corresponds to the assumption that algal loss occurs at a much faster rate than EPS decay ($\delta \gg \eta$). In this limit, the amount of EPS remains at its initial value, $E(t) = E(0) = E_0$. We now analyze the remaining two equations, (4a) and (4b). Setting $\frac{dN}{d\tau'} = \frac{dA}{d\tau'} = 0$, we find two steady-state solutions:

$$p_0 \coloneqq (\frac{a}{b}, 0)$$

$$p_1 \coloneqq \left(\frac{1}{f-1}, \frac{f(af-a-b)}{e^{E_0}c(f-1)}\right).$$

Again, we find a trivial, algae-free solution p_0, as well as a possible nontrivial solution p_1 with persistent algae, provided $\frac{a}{b} > \frac{1}{(f-1)} > 0$, which is necessary to guarantee positive entries in p_1. Evaluating the Jacobian of the matrix differential of (4a)-(4b) at p_0 yields the following eigenvalues (see S2):

$$\lambda_1 = -be^{-E_0}, \lambda_2 = \frac{af-a-b}{a+b}$$

Since λ_1 will always be negative, the stability of p_0 is determined by the sign of λ_2. The sign of λ_2 hinges on the same inequality as the existence of p_1, specifically the relationship between $\frac{a}{b}$ and $\frac{1}{(f-1)}$. If p_1 exists, then p_0 is unstable, since $\frac{a}{b} > \frac{1}{(f-1)}$ and so $\lambda_2 > 0$. If p_1 does not exist, p_0 is stable, since $\frac{a}{b} < \frac{1}{(f-1)}$ and so $\lambda_2 < 0$ (Figure 1).

Turning our attention to the stability of the nontrivial equilibrium, we evaluate the Jacobian at p_1 (see S2):

$$J_{p_1} = \begin{bmatrix} -\frac{e^{-E_0}\left(f^2a-2af+a+b\right)}{f} & -\frac{c}{f} \\ \frac{(af-a-b)e^{-E_0}(f-1)}{c} & 0 \end{bmatrix}$$

We use the trace and determinant to determine stability. If $\frac{a}{b} > \frac{1}{(f-1)}$, then the trace of the Jacobian is negative and the determinant is positive, confirming that p_1 becomes a stable sink for the same values of $\frac{a}{b}$ at which p_0 loses stability (Figure 1). This result echoes our findings in Section 2.1, where we identified a transcritical bifurcation governed by the balance between nutrient inflow and outflow.

We also rule out the possibility of a Hopf bifurcation for this system. For a Hopf bifurcation, the trace of the Jacobian would need to be zero:

$$Trace(J_{p_1}) = 0 \implies f^2a - 2af + a + b = 0 \implies \frac{a}{b} = \frac{-1}{(f-1)^2}$$

which is not possible for nonnegative values of a and b.

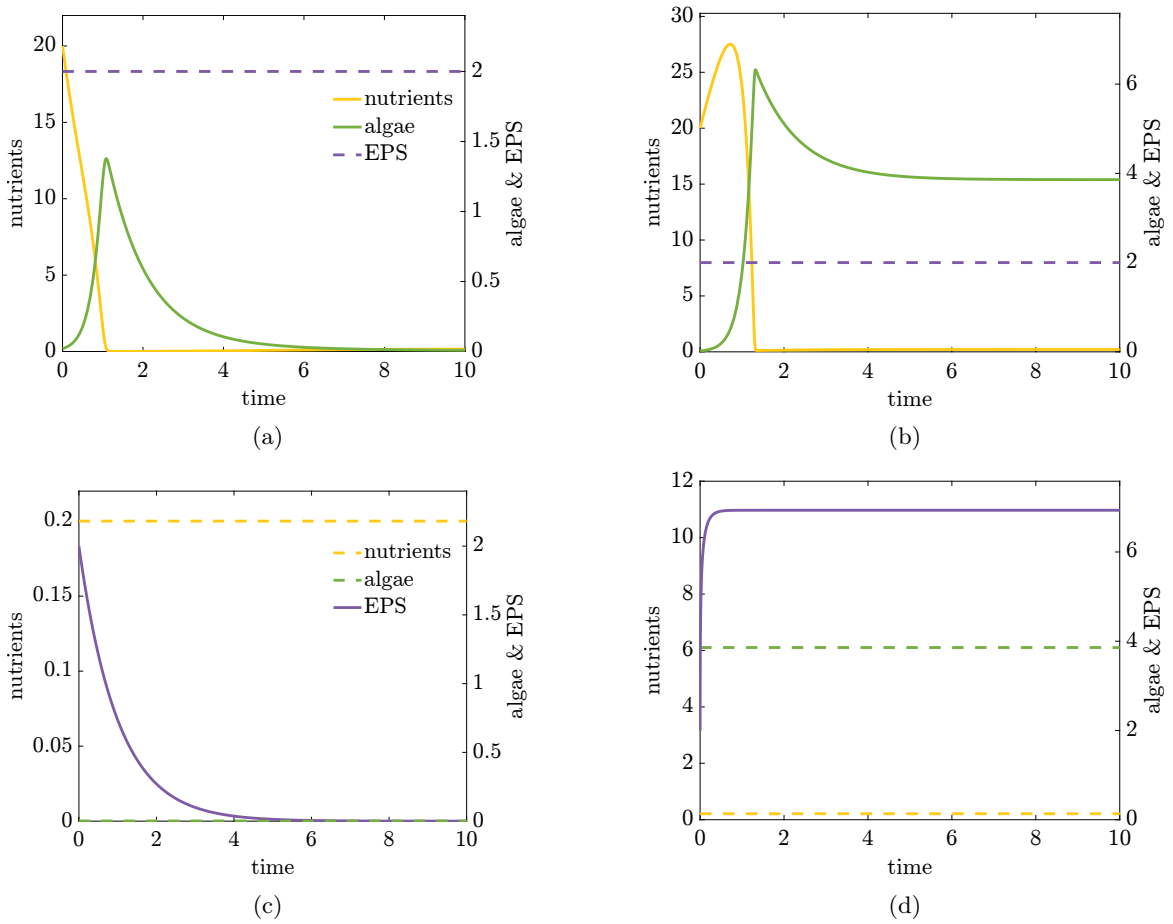

Figure 1: Two possible asymptotic dynamics arise under Regime 1, where we assume EPS dynamics are much slower than algal and nutrient dynamics. In both **(a)** and **(b)**, nutrients and algae evolve on the fast timescale while EPS is held fixed at its quasi-steady state value, ($E = E_0$). In both **(a)** and **(b)**, nutrients and algae are assumed to instantaneously reach their fast quasi-steady state p_0 and p_1, respectively, reducing the system to a single slow EPS equation. In both **(a)** and **(c)**, parameters are such that nutrient loss exceeds nutrient input, resulting in algae and EPS asymptotically approaching 0. Dimensional parameters are as in Table 1, except for $\phi = .0001$ and $\psi = .05$. Corresponding nondimensional parameters are $a = 1.4, b = 7.1, f = 5.7$ thus $\frac{a}{b} < \frac{1}{f-1}$. In both **(b)** and **(d)**, nutrient input is sufficient to sustain algae and EPS asymptotically. Parameters are as in Table 1, here nondimensional parameters $a = 142.9, b = 1.4, f = 5.7$ thus $\frac{a}{b} > \frac{1}{f-1}$.

We now focus on the slow model dynamics of (3b). For this analysis, we do not rescale time, so when we let $\epsilon \to 0$, the left-hand side of the equations in (3a) becomes zero. In this quasi-steady-state limit, we find the same two nutrient and algal equilibria as in the fast system above, p_0 and p_1. In the trivial quasi-steady state p_0, (3b) simplifies to $\frac{dE}{d\tau} = -E$, so the amount of EPS decays exponentially from its initial condition $E(0)$ in the absence of algae. This behavior is biologically reasonable, as no significant amount of new EPS is produced in the absence of algae, and any existing EPS decay. If we instead substitute the nontrivial quasi-steady state p_1 into (3b), we have

$$\frac{dE}{d\tau} = \frac{fd(af - a - b)}{e^E c\,(f-1)} - E. \tag{5}$$

This results in a nontrivial steady-state solution for EPS (Figure 1),

$$E^* = W\left(\frac{fd\,(af - a - b)}{c\,(f-1)}\right)$$

where $W(\cdot)$ is the Lambert W function. The Lambert W function is defined as the solution $W(x)$ to the transcendental equation $We^W = x$ with real domain $x \in [-\frac{1}{e}, \infty)$. Note that in order for $W(\cdot) > 0$ and an equilibrium point E^* to exist, the argument of the Lambert W function is nonnegative, which requires $af - a - b \geq 0$, or equivalently $\frac{a}{b} > \frac{1}{f-1}$. To assess the local stability of E^*, we differentiate the right-hand side of equation (5) with respect to E and evaluate at E^*, which yields:

$$\frac{d}{dE}\left(\frac{dE}{d\tau}\right)|_{E=E^*} = -W\left(\frac{fd(af-a-b)}{c(f-1)}\right) - 1 \tag{6}$$

The stability of E^* is determined by the sign of (6), which depends on $W\left(\frac{fd(af-a-b)}{c(f-1)}\right)$. Since $W(-\frac{1}{e}) = -1$, a change in stability occurs when

$$\frac{fd\,(af-a-b)}{c\,(f-1)} = -\frac{1}{e}. \tag{7}$$

We can reframe this relationship in terms of the ratio of nutrient fluxes, $\frac{a}{b}$,

$$\frac{a}{b} = \frac{-c}{efdb} + \frac{1}{f-1}$$

When $\frac{a}{b}$ is greater than this threshold, then E^* in the slow model is stable (Figure 1).

In the fast model, algae persist when $\frac{a}{b} > \frac{1}{(f-1)}$. Because (5) assumes the same nontrivial algal steady state as in the fast model, if

$$\frac{a}{b} > \frac{1}{f-1} > \frac{-c}{efbd} + \frac{1}{f-1},$$

then, algae in the fast model will rapidly reach a nontrivial steady state, with a corresponding nontrivial EPS steady state in the slow model. This fast-slow analysis reveals dynamics consistent with our previous findings: if nutrient input rates are sufficiently high relative to nutrient loss, the system can sustain positive algae and EPS concentrations asymptotically.

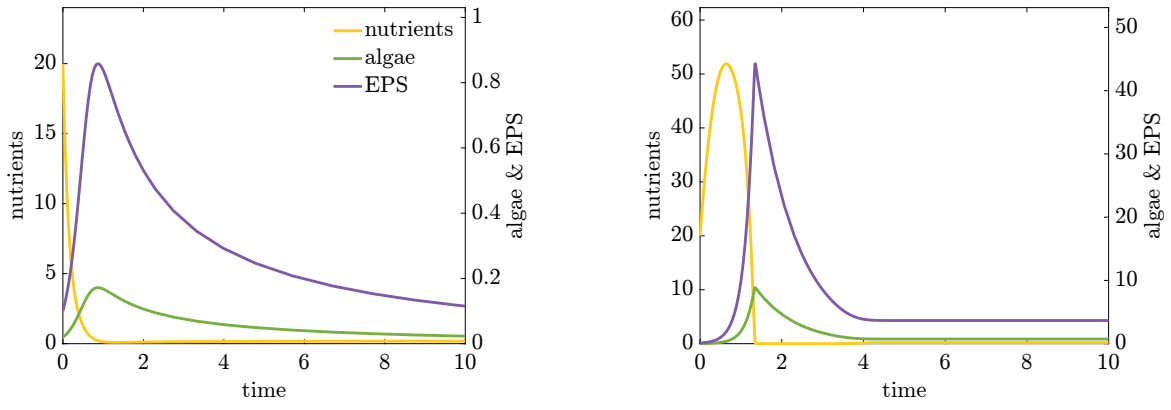

Figure 2: Two possible asymptotic regimes under Regime 2, arising from timescale separation in which EPS dynamics track algal dynamics. In this regime, EPS adjusts on the same fast timescale as algal and nutrient dynamics. In both **(a)** and **(b)**, parameter values transition from a regime in which nutrient loss exceeds nutrient input ($\frac{a}{b} < \frac{1}{f-1}$), resulting in algal extinction and stability of the trivial equilibrium p_0, to a regime in which nutrient input dominates loss ($\frac{a}{b} > \frac{1}{f-1}$), yielding a stable positive algal equilibrium p_1. **(a):** Dimensional parameters are as in Table 1, except for $\phi = .0001$ and $\psi = .05$. for the left column. Here, nondimensional parameters are $a = 1.4, b = 7.1, f = 5.7$ thus $\frac{a}{b} < \frac{1}{f-1}$. **(b):** Parameters are as in Table 1, here, nondimensional parameters $a = 142.9, b = 1.4, f = 5.7$ thus $\frac{a}{b} > \frac{1}{f-1}$.

2.2.2 Regime 2: EPS dynamics are fast, responding instantaneously to changes in algal biomass

In the previous section, we considered a possible regime where EPS dynamics are much slower than those of nutrients and algae. Here, we consider the implications of the opposite extreme: EPS responds instantaneously to changes in nutrient and algae levels. Mathematically, we model this by assuming EPS perfectly tracks algae, so $E(t) = \sigma A(t)$, where σ is a scaling term. Under this assumption, model (2) becomes

$$\begin{aligned} \frac{dN}{dt} &= \phi e^{-\frac{\sigma A}{\mu}} - \frac{\nu N}{\gamma + N} A - \psi e^{-\frac{\sigma A}{\mu}} N \\ \frac{dA}{dt} &= \xi \frac{\nu A N}{\gamma + N} - \delta A \\ E(t) &= \sigma A(t). \end{aligned} \tag{8}$$

Nondimensionalizing the system (Appendix 8) yields:

$$\begin{aligned} \frac{dN}{dt} &= a e^{-hA} - \frac{cNA}{N+1} - bNe^{-hA} \\ \frac{dA}{dt} &= \frac{fNA}{N+1} - A \\ E(t) &= hA \end{aligned} \tag{9}$$

We ignore $E(t)$ in our analysis, since $E(t)$ dynamics are directly proportional to $A(t)$. This system again has two steady-state solutions for N and A:

$$r_0 = \left(\frac{a}{b}, 0\right)$$
$$r_1 = \left(\frac{1}{f-1}, \frac{W\left(hf\frac{(af-a-b)}{c(f-1)}\right)}{h}\right),$$

corresponding to a trivial, algae-free steady state r_0, and a nontrivial steady state r_1 with persistent algae (and thus persistent EPS at concentration $E^* = hA^*$).

Evaluating the Jacobian of the matrix differential equation of (9) at r_0 yields the following eigenvalues (see S3):

$$\lambda_1 = -b, \quad \lambda_2 = \frac{af - a - b}{a + b}.$$

λ_1 is always negative, so the stability of r_0 is determined by the sign of λ_2. As in Section 2.2.1, we find that r_0 loses stability through a transcritical bifurcation at $\frac{a}{b} = \frac{1}{(f-1)}$, demonstrating the importance of nutrient fluxes in sustaining persistent algal communities.

Observe that this transcritical bifurcation occurs exactly at the point where the entries of r_1 become nonnegative.

Due to the presence of the Lambert W function, analyzing the stability of r_1 is not as straightforward as evaluating the Jacobian of (9) at r_1. Instead, we proceed as follows. First, we substitute $N^* = \frac{1}{f-1}$ into (9) to obtain an expression for A^* as a function of system parameters:

$$\frac{dN}{dt} = a\mathrm{e}^{-hA^*} - \frac{cA^*}{f} - \frac{b\mathrm{e}^{-hA^*}}{f-1} = 0.$$

We can then rearrange this expression in terms of one of our parameters, here chosen to be b, the physical nutrient loss rate,

$$b = (f-1)(a - cA^*\mathrm{e}^{hA^*}/f). \tag{10}$$

Plugging this expression into both $\frac{dN}{dt}$ and $\frac{dA}{dt}$ in (9), we can evaluate the Jacobian of (9), finding the determinant and trace as functions of A^* (see S3):

$$Det(J_{r_1}) = \frac{(hA^* + 1)\, cA^* \,(f-1)^2}{f^2} \tag{11}$$

$$Tr(J_{r_1}) = \frac{(f-1)\left(-\mathrm{e}^{-hA^*} a\, f^2 + cA^*\right)}{f^2} \tag{12}$$

The determinant is always nonnegative, and it can be proven that the trace is always negative (Appendix 8), so this equilibrium is stable.

Next, we ask whether a Hopf bifurcation could occur by examining the condition $Tr(J_{r_1}) = 0$. Setting the trace to zero in (12) gives:

$$cA^* = af^2 e^{-ha}$$

Substituting this term into the expression for b in equation (10), we compute:

$$\begin{aligned} sign(b) &= sign(-cA^* + afe^{-hA^*}) \\ &= sign(-af^2 e^{-hA^*} + afe^{-hA^*}) \\ &= sign(-afe^{-hA^*}(f+1)) \\ &< 0 \end{aligned}$$

Again, we see that achieving $Tr(J_{r_1}) = 0$ requires $b < 0$, which is biologically implausible. Hence, for all positive parameter values, $Tr(J_{r_1}) < 0$, and the equilibrium point r_1 is a stable sink (Figure 2).

2.2.3 Regime 3: EPS dynamics occur over similar timescales to those of algae and nutrients

The final regime explores the hypothesis that EPS dynamics occur on a timescale similar to that of algae and nutrients, requiring us to consider the full system of three ordinary differential equations in (2). We have already nondimensionalized this model in (3), and we now analyze the full system dynamics rather than making a quasi-steady-state assumption, as was done in Section 2.1. The steady states (N^*, A^*, E^*) of (3) are:

$$\begin{aligned} q_0 &= \left(\frac{a}{b}, 0, 0\right) \\ q_1 &= \left(\frac{1}{f-1}, \frac{1}{d} W\left(\frac{(af-a-b)fd}{c(f-1)}\right), W\left(\frac{(af-a-b)fd}{c(f-1)}\right)\right) \end{aligned}$$

Notice the similarity to the equilibria p_0 and p_1 in Regime 1 (Section 2.2.1) and r_0 and r_1 in Regime 2 (Section 2.2.2). As in Section 2.2.2, the nontrivial EPS steady state is a scalar multiple of the algal steady state. Note that N^* in q_1 is only plausible if $f \geq 1$. As above in Regime 1 (Section 2.2.1), this transcritical bifurcation occurs exactly at the point where the Lambert W entries of q_1 become nonnegative.

To determine the stability of q_0, we examine the eigenvalues of the Jacobian of (3) at q_0, (see S4):

$$\lambda_1 = -1, \lambda_2 = -b, \lambda_3 = \frac{af-a-b}{a+b}.$$

As in the previous two regimes, the trivial steady state q_0 is stable if $\frac{a}{b} < \frac{1}{(f-1)}$, and it is the ratio of nutrient input to loss that determines algal persistence (Figure 3).

We next examine the stability of q_1, where algae and EPS persist. Numerical bifurcation diagrams suggest that immediately following the transcritical bifurcation, the nontrivial steady state q_1 is a stable spiral, and that increasing nutrient input far enough leads not only to persistent algae and EPS but may eventually result in periodic dynamics through a Hopf bifurcation (Figure 3). Motivated by these numerical findings, we look for two bifurcations: one where the eigenvalues of the Jacobian evaluated at the nontrivial fixed point become negative, signifying the stability of q_1; and one where a complex conjugate pair of eigenvalues becomes purely imaginary, signifying periodic asymptotic dynamics.

In sections 2.2.1 and 2.2.2, the system was two-dimensional, allowing stability to be determined from the trace and determinant of the Jacobian. In the full three-dimensional model, this approach is no longer sufficient. Moreover, q_1 involves the Lambert W function, which makes direct substitution

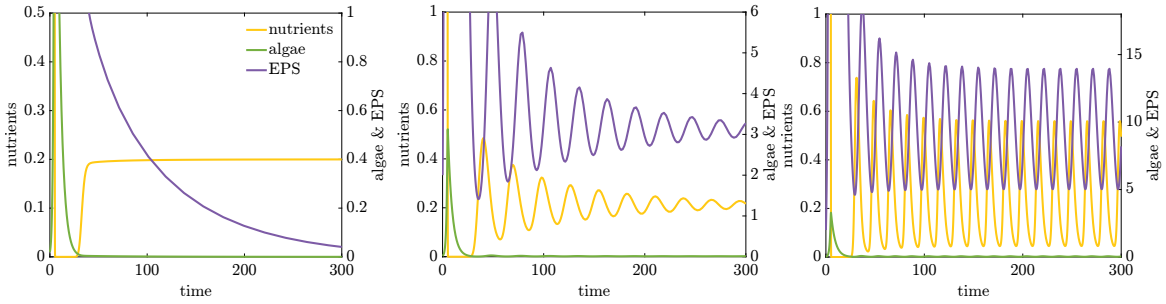

Figure 3: Three possible asymptotic behaviors under Regime 3, arising from the ratio of nutrient inflow to nutrient outflow. **(a):** When the ratio of nutrient input to loss is too low ($\frac{a}{b} < \frac{1}{f-1}$), then the system is asymptotically free from algae and EPS (q_0 is stable). Parameters are as in Table 1, except $\phi = .0001$ and $\psi = .05$ which corresponds to nondimensional parameters $a = 1.4$, $b = 71.4, f = 5.7$. **(b):** As $\frac{a}{b}$ increases and crosses the transcritical bifurcation threshold, we get a stable spiral towards the nontrivial equilibrium, q_1. Note that algae are also oscillatory here, but difficult to see due to the low levels at these parameter values. Parameters are as in Table 1, except $\phi = .0001$ and $\psi = .001$ with nondimensional parameters $a = 1.4$, $b = .14, f = 5.7$. **(c):** When (a, b) is on the right side of the manifold (Figure 4), we get a limit cycle around equilibrium point q_1. As in the middle figure, algae are oscillatory here, though difficult to see. Here, parameters are as in Table 1.

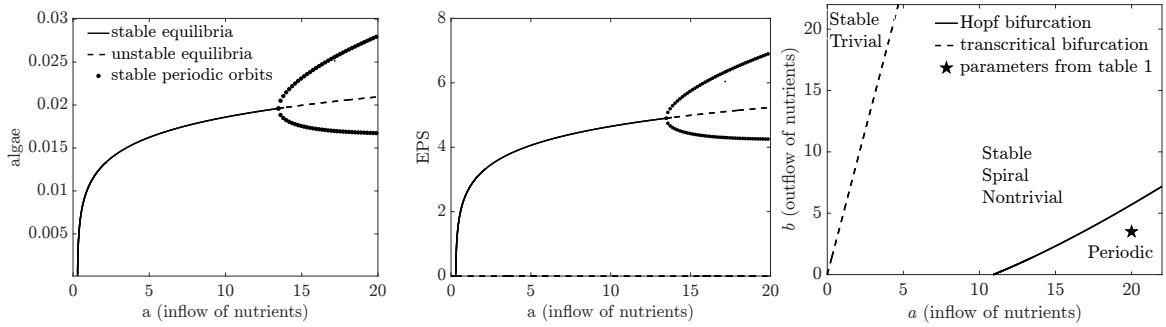

Figure 4: Bifurcation diagrams for regime 3. **(a):** Bifurcation diagram of asymptotic algal biomass, A. **(b):** Bifurcation diagram of asymptotic EPS concentration, E. **(c):** Bifurcation diagram of both inflow of nutrients, a, and outflow of nutrients, b. For values of a slightly larger than 0, a transcritical bifurcation occurs in which the trivial equilibrium loses stability and a stable nonzero equilibrium emerges. As a increases further, the nontrivial equilibrium undergoes a Hopf bifurcation, giving rise to stable periodic oscillations. Parameters are as in Table 1.

into the Jacobian algebraically cumbersome. For this reason, we instead work symbolically with the Jacobian and impose steady-state relationships later in the calculation, thereby avoiding explicit Lambert W terms.

To explore the possibility of a periodic solution, we construct the full Jacobian J_{q_1}, evaluate it at the fixed point q_1 (see S4), and analyze its eigenvalues. We construct a modified characteristic polynomial, $p_{char} = det(J_{q_1} - i\sqrt{\omega}I)$, where $i\sqrt{\omega}$ are the purely complex eigenvalues of the system. The roots of the characteristic polynomial may contain both real and imaginary parts. At a Hopf bifurcation, we require both parts to vanish simultaneously. Therefore, we set $R = Re(p_{char}) = 0$ and $Im(p_{char}) = 0$. We first solve $Im(p_{char}) = 0$, which gives an expression for ω (see S4). Next, we consider $Re(p_{char}) = 0$, but solving this equation directly for ω is challenging because the state variables N, A, and E appear in the expression. To address this challenge, we impose the steady-state conditions from the nondimensional system (3), so

$$E^* = dA^*$$

and

$$N^* = \frac{1}{f-1}.$$

Substituting these terms into the differential equation for $\frac{dN}{dt}$ yields an expression that depends on several parameters and the state variable A:

$$\frac{dN}{dt} = \frac{f(af-a-b)e^{-dA^*} - cA^*(f-1)}{f(f-1)}.$$

Setting $\frac{dN}{dt} = 0$ gives the steady state relationship between parameters and A,

$$b = -\frac{(f-1)(cA^*e^{dA^*} - af)}{f}.$$

Now, with both ω and b expressed analytically (See S4), we can find the solutions to $Re(p_{char}) = 0$. We choose to express these solutions in terms of a, maintaining our interest in how nutrient fluxes shape system dynamics. The parameter a appears quadratically in $Re(p_{char})$, and we find a pair of solutions: one positive and one negative. The negative root is irrelevant, so the remaining solution gives an analytical expression for a as a function of several parameters and A^* (see S4). Together, these expressions for a and b describe a Hopf bifurcation manifold that determines whether the nontrivial steady state is stable or whether there is a stable periodic orbit around it (Figure 4).

2.3 Comparison between biological regimes

Regime	**Trivial steady state** (N^*, A^*, E^*)	**Stability Condition**	**Nontrivial steady state** (N^*, A^*, E^*)	**Hopf Bifurcation**
Regime 1	$(\frac{a}{b}, 0, 0)$	$\frac{a}{b} < \frac{1}{f-1}, (f > 1)$	$\left(\frac{1}{f-1}, \frac{f(af-a-b)}{e^{E_0}c(f-1)}, W\left(d\frac{f(af-a-b)}{c(f-1)}\right)\right)$	N/A
Regime 2	$(\frac{a}{b}, 0, 0)$	$\frac{a}{b} < \frac{1}{f-1}, (f > 1)$	$\left(\frac{1}{f-1}, \frac{1}{h}W\left(h\frac{f(af-a-b)}{c(f-1)}\right), hA^*\right)$	N/A
Regime 3	$(\frac{a}{b}, 0, 0)$	$\frac{a}{b} < \frac{1}{f-1}, (f > 1)$	$\left(\frac{1}{f-1}, \frac{1}{d}W\left(d\frac{f(af-a-b)}{c(f-1)}\right), dA^*\right)$	Figure 4

Table 2: Summary comparing asymptotic model behavior across regimes.

Across all three regimes, the trivial steady state, without persistent algae or EPS, is stable when the ratio of nutrient inflow to nutrient loss is too small (i.e. $\frac{a}{b} < \frac{1}{f-1}$ for $f > 1$) (Table 2). In this case, nutrient inflow a is too low to offset physical and biological losses (captured in b, the nutrient loss rate, and f, the algal nutrient uptake rate), preventing algal establishment and resulting in EPS production. Conversely, when nutrient inputs are sufficiently high relative to loss $\left(\frac{a}{b} > \frac{1}{f-1}\right)$, algae persist, with resulting sustained EPS production.

The parameters h and d seen in the nontrivial steady state in Regimes 2 and 3 (Table 2) share the same units, and both represent the growth rate of EPS. In Regime 2, the parameter σ represents the efficiency with which algal biomass is converted into EPS, setting the proportionality between algal growth and EPS accumulation. Larger values of σ correspond to more rapid EPS production per unit of algal biomass, while smaller values indicate weaker coupling between algal growth and EPS synthesis. When σ is set to $\sigma = \frac{\rho}{\eta}$, where ρ is the production rate of EPS and η is the degradation of EPS, then $d = h$, leading to identical steady-state behavior in Regimes 2 and 3. In both of these regimes, EPS concentration is directly proportional to algal biomass at steady state.

Based on the parameters found in the literature (Hunke et al. (2024); Krembs et al. (2011)), we have $E^* = dA^* > A^*$, indicating that $d, h > 1$. Therefore, in both Regimes 2 and 3, the nontrivial equilibrium EPS concentration exceeds the corresponding algal biomass, consistent with observational studies (Stoecker et al. (2000)).

To compare the nontrivial algal steady states across the different regimes in Table 2, we begin with the expression

$$x = \frac{f(af - a - b)}{c(f-1)} > 0$$

which appears in each regime's nontrivial steady state A^*. First, we compare the value of Regime 1, xe^{-E_0}, to that of Regime 2, $\frac{1}{h}W(hx)$. To determine which is larger, we find when $\frac{1}{h}W(hx) = xe^{-E_0}$. Solving for x yields $x = \frac{E_0 e^{E_0}}{h}$.

When $0 < x < \frac{E_0 e^{E_0}}{d}$, the nontrivial steady-state algal biomass in Regime 2 exceeds that in Regime 1, i.e., $A_2^* > A_1^*$. At the threshold value $x = \frac{E_0 e^{E_0}}{d}$, the two regimes yield identical steady-state algal biomass, so that $A_1^* = A_2^*$. For $x > \frac{E_0 e^{E_0}}{d}$, the ordering reverses, and Regime 1 supports a larger asymptotic algal biomass than Regime 2, i.e., $A_1^* > A_2^*$. An identical comparison holds for Regime 3, as its expression for A^* differs from that of Regime 2 only by replacing h with d, leading to the same conclusions regarding the relative magnitudes of the nontrivial steady states. Finally, if $E_0 > 0$, the quantity $\frac{x}{e^{E_0}} < x$ indicates that regime 1 yields less asymptotic algal biomass than the unmodified baseline value x; in this case, EPS reduces the nontrivial steady state algal concentration A^*.

In summary, the comparison across regimes reveals a clear hierarchy governed by a threshold $x = \frac{E_0 e^{E_0}}{d}$: Below this threshold, Regimes 2 and 3 support higher asymptotic algal biomass than Regime 1, while above it, the ordering reverses. Regime 2 serves as an intermediate case, aligning with Regime 3 when $d = h$ and shifting otherwise. In all cases, EPS reduces steady-state algal biomass relative to the baseline value x, with the magnitude of this reduction depending on EPS production parameters.

2.4 Transient bloom dynamics

In addition to studying the asymptotic behavior of algae and EPS, we are also interested in their transient dynamics during an algal bloom. Transient dynamics occur over shorter, often ecologically important time scales. Our transient analysis is inspired by that of Huppert (2002), who explored transient bloom dynamics for a classic model of nutrient-driven phytoplankton blooms (Huppert et al. (2002)). The relative simplicity of that model allowed for an analytic analysis of the transient dynamics (Huppert et al. (2002)). Adding EPS to the nutrient-algae system precludes the use of those analytic approaches, so we instead numerically investigate the dependence of the bloom dynamics on initial conditions, nutrient fluxes, and EPS accumulation and decay rates. To quantify these effects, we conducted a local sensitivity analysis to determine the parametric dependencies of the maximum nutrient, algal, and EPS concentrations (N_{max}, A_{max}, and E_{max}) during the algal bloom. We focus our transient analysis on the model under Regime 3, which makes no strong assumptions about the timescale of EPS dynamics.

Note that we define a "bloom" as occurring whenever there is an initial increase in algae immediately following time $t = 0$. Mathematically, this requires $\frac{dA}{dt}|_{t=0} > 0$, which necessitates $N_0 > \frac{1}{f-1}$ in (3). In what follows, we assume N_0 is above this threshold, resulting in an initial increase in $A(t)$. We then vary parameters by 50-150% in the dimensional model (2) around the values in Table 1.

Influence of nutrient fluxes on bloom peaks

Previous work on nutrient-driven phytoplankton dynamics suggests that an increase in the nutrient inflow rate leads to higher phytoplankton and nutrient peaks (Huppert et al. (2002)), and vice versa for the nutrient loss rate. Consistent with these findings, we observe that increasing ϕ results in higher maximum concentrations of algae (A_{max}), nutrients (N_{max}), and EPS (E_{max}), while increasing ψ lowers them (Figure 5).

Influence of algal growth and loss rates on bloom peaks

As the nutrient uptake rate of bottom-ice algae, ν, increases, N_{max} decreases, while A_{max} and E_{max} both increase, as one may have intuitively expected (Figure 5). Similarly, decreasing the nitrogen half-saturation constant, γ, should increase the rate of nutrient uptake by algae, but within the tested range γ has little effect on bloom peaks (Figure 5). In contrast, increasing the algal mortality rate, δ, produces the expected effect: both $A_{\max}$ and E_{max} decline, while N_{max} remains largely unchanged

(Figure 5). Finally, increasing the chl-a to nitrogen conversion ratio, ξ, increases both algal and EPS peaks, accompanied by a slight reduction in the nutrient maximum (Figure 5).

Influence of EPS accumulation and loss rates on bloom peaks

EPS influences bloom dynamics in ways consistent with the hypothesized EPS-mediated feedback mechanism. Increasing the EPS production rate ρ leads to a higher maximum EPS concentration (E_{max}), while reducing the peak of the algal bloom (A_{max}) (Figure 5). Similarly, increasing the degradation rate of EPS η causes E_{max} to decrease while N_{max} and A_{max} increase (Figure 5). These inverse relationships between peak EPS accumulation and peak bloom intensity suggest that the negative EPS-mediated biophysical feedback, which is the focus of this paper, reduces peak algal concentrations, in addition to the reduction in asymptotic algal concentrations explored earlier.

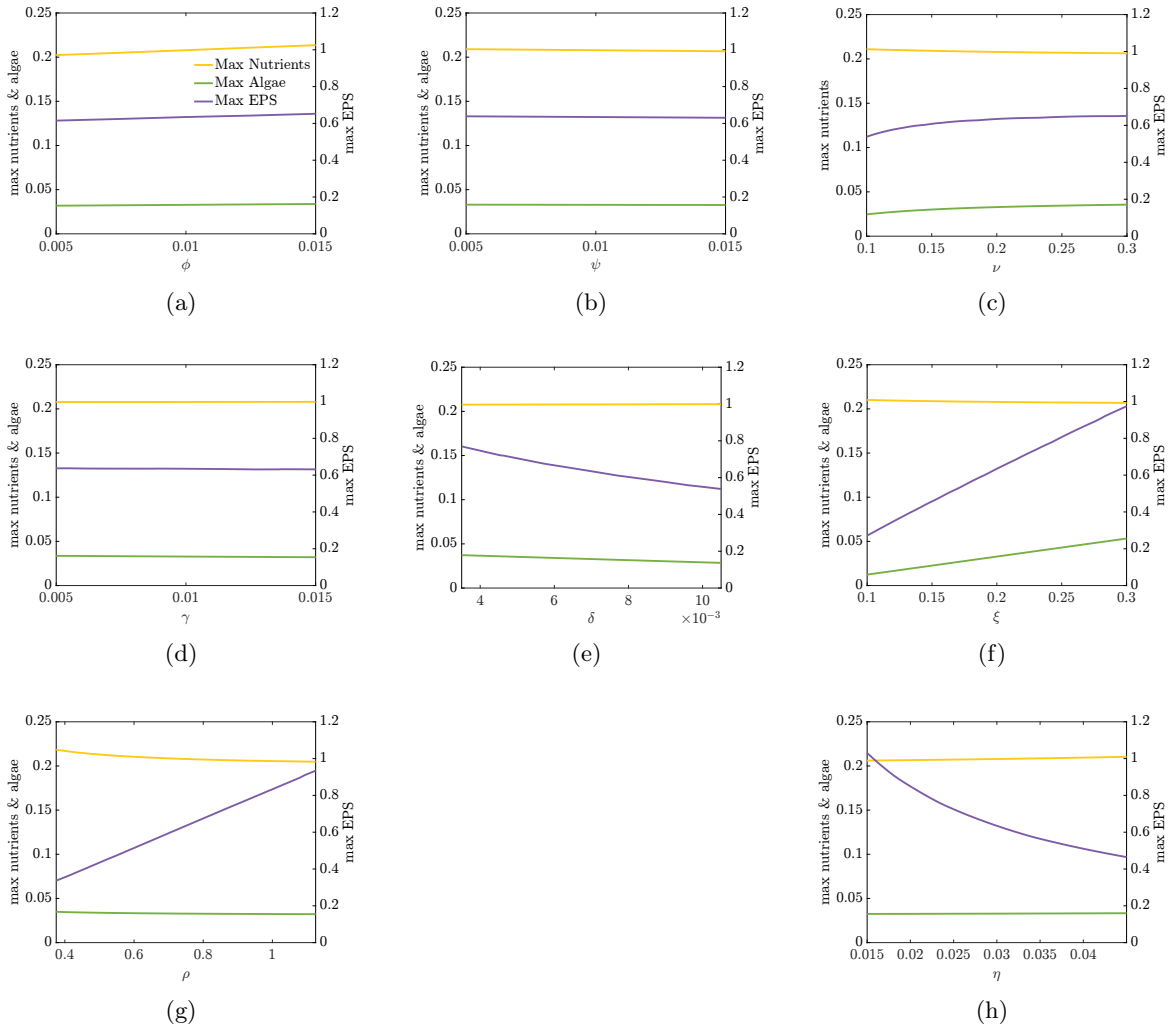

Figure 5: Each graph represents the effects that each parameter has on the nutrient, algal, and EPS concentration peaks ($N_{max}, A_{max}, E_{max}$ respectively). Parameter values vary between 50% and 150% of the values in Table 1. In contrast to the other figures, the algal peak A_{max} is plotted on the left y-axis (rather than the right y-axis) to show its variation more clearly.

3 Real world model implications

We selected parameter values consistent with observations in polar sea ice systems (Table 1). These values include both empirically measured quantities and reasonable estimates derived from biogeochemical literature, and are intended to represent plausible conditions encountered within sea ice.

Figure 6 shows the solution of model 2 using the parameter values in Table 1. Here we see that high nutrient concentrations initially support rapid algal growth and subsequent EPS production. Eventually, as nutrients are depleted, the bloom ends and the system transitions to a nutrient-limited state (Collins et al. (2008); Krembs et al. (2002)).

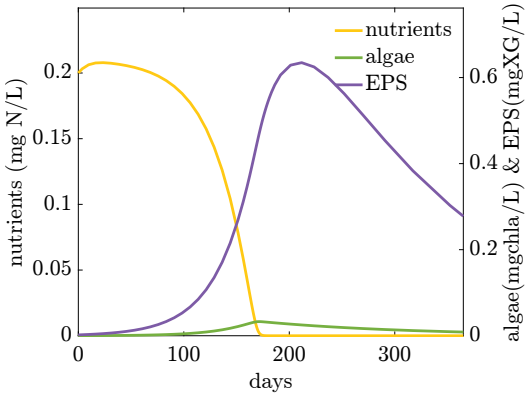

Figure 6: Time series of nutrients, algae, and EPS over the first simulated year. Algal biomass and EPS persist while nutrient concentrations are gradually depleted to a sustained level, consistent with observations found from Arctic sea ice ecosystems. The modeled concentrations of nutrients, algae, and EPS during a bloom fall within reported ranges in the literature, indicating a realistic parameterization. However, the duration of the simulated algal bloom happens later than typically observed in field studies. Parameter values are as in Table 1.

4 Discussion

In this paper, we extended a classic nutrient-algae model to include EPS-mediated biophysical feedbacks. We considered three regimes to distinguish between possible timescales of EPS dynamics. All regimes share two asymptotic scenarios: one in which EPS, algae, and nutrients persist, and another in which, despite sustained nutrient availability, algae and EPS do not persist. Notably, the shift between these two asymptotic states depends only on a combination of the nutrient fluxes and the growth rate of algae; the bifurcation is unrelated to EPS dynamics, and is consistent with the bifurcation found in the nutrient-phytoplankton model, without EPS (Huppert et al. (2002)). In all regimes, reductions in permeability caused by EPS accumulation lead to lower asymptotic nutrient availability, ultimately suppressing algal growth and altering system stability. When the feedback is sufficiently strong, this results in periodic oscillations in nutrients, algae, and EPS, highlighting the role of EPS in determining whether the system approaches a steady state or oscillatory behavior. Thus, across regimes, the system's qualitative behavior remains consistent, even as the quantitative solutions differ slightly. This robustness suggests that the essential feedback mechanics governing EPS and algal interactions are preserved regardless of the timescale assumptions on EPS. Analysis of model transient dynamics revealed that EPS-mediated biophysical feedbacks also reduce bloom intensity, suggesting that these feedbacks have both short and long-term implications for primary productivity within the ice.

Perhaps the most salient unknown in our models is which functional form best describes the effects of EPS on nutrient fluxes. In addition to the exponential form analyzed here, we also considered an alternate, Hill function for the nutrient flux terms ($\alpha(E)$ and $\beta(E)$) (Appendix 8). This analysis demonstrates that varying the feedback strength encoded by the Hill function can qualitatively alter the system's dynamics, including the emergence of a Hopf bifurcation that is absent under weaker feedback. Future empirical and modeling studies are needed to improve our confidence in the functional forms for $\alpha(E)$ and $\beta(E)$.

While our asymptotic analyses suggest EPS suppresses asymptotic algal concentrations and may even cause periodic solutions, real sea ice ecosystems are governed by significant additional complexities such as seasonal temperature fluctuations. These temperature swings shape ice and snow dynamics, which determine the amount of light available for photosynthesis within the ice and the availability and stability of the ice substrate as an algal habitat (Riedel et al. (2006)). Additional

biological interactions, including those with bacteria, heterotrophic grazers, and viruses, as well as competition with other organisms for light and nutrients, introduce further complexity not considered here. Future modeling efforts could merge models of these more complex dynamics with the EPS-mediated feedbacks explored here.

This modeling study represents a novel approach to integrating dynamic sea-ice biology and physics at the microscale. Previous studies have treated these processes independently, focusing on either sea ice biogeochemistry or physics within sea ice (Lannuzel et al. (2020); Miller et al. (2015); Roukaerts et al. (2021); Tedesco and Vichi (2014)). This study is, to the best of our knowledge, the first to quantitatively investigate the influence of EPS on sea ice permeability and the resulting impacts on algal growth. The EPS-mediated feedbacks explored here suppressed algal biomass both during the bloom and asymptotically, while simultaneously reducing ice permeability, highlighting the tight coupling between sea ice permeability and biological productivity.

5 Supporting information

All supplemental information, analysis, and code used to generate all figures are available in a GitHub repository. A corresponding DOI will be created following acceptance for publication.

6 Author contributions

ARJ led all aspects of the study, including model development, analysis, and manuscript preparation. JRR contributed substantially to the study's conceptualization and to the initial manuscript draft. All other authors contributed to model formulation, manuscript editing and revisions. ARJ acknowledges the use of an AI-based language tool solely for editing and polishing the manuscript text (spelling, grammar, and general style).

7 Acknowledgments

ARJ gratefully acknowledges support from the University of Utah Department of Mathematics and the U.S. National Science Foundation through Grant DMS-2136198. KMG gratefully acknowledges support from the US National Science Foundation through grants DMS-2136198 and DMS-2206171, and the Applied and Computational Analysis Program at the US Office of Naval Research through grants N00014-21-1-2909 and N00014-26-1-2114.

8 Declerations

Competing Interests The authors declare that they have no financial or non-financial interests that are directly or indirectly related to the work submitted for publication.

Appendix A: Hill functional form

Based on our findings above that EPS-mediated feedback can result in periodic solutions, we now ask what level of negative feedback is required for the system to exhibit this periodic behavior. To explore the impacts of an alternative functional choice for the nutrient flux terms, we introduce an alternative functional form for $\alpha(E)$ and $\beta(E)$. The Hill function captures saturation effects by modeling how increasing EPS diminishes feedback strength on nutrient inflow and outflow. This reflects some intuition that, beyond a certain concentration, additional EPS may have little additional impact on nutrient dynamics. We set $\alpha(E) = \frac{\phi}{(1+\mu E)^p}$ and $\beta(E) = \frac{\psi}{(1+\mu E)^p}$ in (1), where p controls the level of negative feedback. Nondimensionalization yields

$$\epsilon \frac{dN}{dt} = \frac{a}{(1+E)^p} - \frac{cNA}{1+N} - \frac{bN}{(1+E)^p} \tag{13a}$$

$$\epsilon \frac{dA}{dt} = \frac{fNA}{1+N} - A \tag{13b}$$

$$\frac{dE}{dt} = dA - E \tag{13c}$$

Note that the system is nondimensionalized with the same parameters as before (see S6) to aid in interpretation. This system, like the previous ones, has a trivial and nontrivial equilibrium,

$$g_0 = (\frac{a}{b}, 0, 0)$$

$$g_1 = \left(\frac{1}{f-1}, \frac{\left(\frac{c}{f-1} - a\right)\left(1 + \frac{1}{f-1}\right)}{(E+1)^p \left(\frac{c}{f-1}\right)}, Ad \right)$$

We evaluate the Jacobian of (13) at g_0 and find the eigenvalues:

$$\mu_1 = -1, \mu_2 = -b, \mu_3 = \frac{fa - a - b}{b + a}.$$

As before, the stability of the trivial solution g_0 is lost when $\frac{a}{b} > \frac{1}{f-1}$.The remaining stability analysis continues to follow the analysis of Section 2.2.3 (see S6). We highlight here how the results of model (13) differ from those of model (2), which had exponential terms for $\alpha(E)$ and $\beta(E)$. In this model, we can vary p, the strength of the EPS-mediated feedback in the system, and as we do so, a Hopf bifurcation emerges (Figure A1), suggesting that a stronger feedback induces periodic behavior.

Exploring this relationship further, we see that a higher nutrient inflow promotes oscillations, but only if the negative feedback is not too strong. As feedback strength increases, less nutrient inflow is needed to induce a Hopf bifurcation. This result suggests that EPS can destabilize or stabilize the system depending on how strongly EPS feeds back on nutrient dynamics (Figure A1).

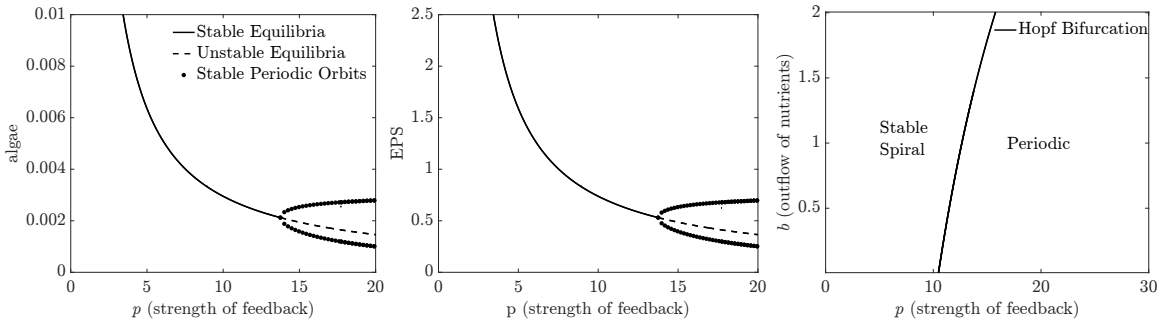

(a) (b) (c)

Figure A1: **(a):** Algal bifurcation diagram of feedback strength p showing that as p increases a periodic solution appears.**(b):** EPS bifurcation diagram of feedback strength p showing that as p increases a periodic solution appears **(c):** Two-parameter bifurcation graph. On one side of the curve, there is a stable spiral towards the equilibrium point g_1, while on the other side, there is a periodic orbit around g_1. All parameter values are as in Table 1.

Appendix B: Regime 2 trace is always negative

We show here that the trace $Tr(J_{r_1})$ in (12) is negative by proof by contradiction. Assume both $b > 0$ and $Tr(J_{r_1}) > 0$. Then it follows from (10) that $\text{sign}(b) = \text{sign}(afe^{-hA^*} - cA^*)$ and the $\text{sign}(Tr(J_{r_1}))$ =$\text{sign}(-\text{e}^{-hA^*} a\, f^2 + cA^*)$ from equation (12). Using the fact that $b > 0$ and $Tr(J_{r_1}) > 0$ gives:

$$afe^{-hA^*} > cA^* > af^2e^{-hA^*}$$
$$\implies f > \frac{cA^*}{ae^{-hA^*}} > f^2$$

However, assuming that $f > 1$ implies that $f^2 > f$, contradicting the inequality $f > f^2$. Thus, there is no regime where both $Tr(J_{r_1}) > 0$ and $b > 0$. Thus, $Tr(J_{r_1}) > 0 \implies b < 0$, which lies outside the biologically meaningful parameter regime.

Appendix C: Nondimensional parameters for regime 1 and 3

$$\begin{aligned} N^* &= \frac{N}{\gamma} & a &= \frac{\phi}{\gamma\delta} \\ A^* &= \frac{A}{\gamma} & b &= \frac{\psi}{\delta} \\ E^* &= \frac{E}{\mu} & c &= \frac{\nu}{\delta} \\ t &= \frac{\tau}{\eta} & d &= \frac{\rho\gamma}{\mu\eta} \\ f &= \xi c & \epsilon &= \frac{\eta}{\delta} \end{aligned}$$

Appendix D: Nondimensional parameters for regime 2

$$
\begin{aligned}
N^* &= \frac{N}{\gamma} & a &= \frac{\phi}{\gamma\delta} \\
A^* &= \frac{A}{\gamma} & b &= \frac{\psi}{\delta} \\
t &= \frac{\tau}{\delta} & c &= \frac{\nu}{\delta} \\
f &= \xi c & h &= \frac{\sigma\gamma}{\mu}
\end{aligned}
$$

References

Arrigo KR, Van Dijken G, Pabi S (2008) Impact of a shrinking Arctic ice cover on marine primary production. Geophysical Research Letters 35(19):L19603. https://doi.org/10.1029/2008GL035028

Brown TA, Galicia MP, Thiemann GW, et al (2018) High contributions of sea ice derived carbon in polar bear (Ursus maritimus) tissue. PLOS ONE 13(1):e0191631. https://doi.org/10.1371/journal.pone.0191631

Collins RE, Carpenter SD, Deming JW (2008) Spatial heterogeneity and temporal dynamics of particles, bacteria, and pEPS in Arctic winter sea ice. Journal of Marine Systems 74(3–4):902–917. https://doi.org/10.1016/j.jmarsys.2007.09.005

Ewert M, Deming JW (2013) Sea ice microorganisms: Environmental constraints and extracellular responses. Biology 2(2):603–628. https://doi.org/10.3390/biology2020603

Gradinger R (2009) Sea-ice algae: Major contributors to primary production and algal biomass in the Chukchi and Beaufort Seas during May/June 2002. Deep Sea Research Part II: Topical Studies in Oceanography 56(17):1201–1212. https://doi.org/10.1016/j.dsr2.2008.10.016

Hunke E, Allard R, Bailey DA, et al (2024) CICE-Consortium/Icepack: Icepack 1.5.0. https://doi.org/10.5281/zenodo.14188409

Huppert A, Blasius B, Stone L (2002) A Model of Phytoplankton Blooms. The American Naturalist 159(2):156–171. https://doi.org/10.1086/324789

Kim K, Ha S, Kim BK, et al (2020) Carbon and nitrogen uptake rates and macromolecular compositions of bottom-ice algae and phytoplankton at Cambridge Bay in Dease Strait, Canada. Annals of Glaciology 61(82):106–116. https://doi.org/10.1017/aog.2020.17

Krembs C, Eicken H, Junge K, et al (2002) High concentrations of exopolymeric substances in Arctic winter sea ice: Implications for the polar ocean carbon cycle and cryoprotection of diatoms. Deep-Sea Research Part I: Oceanographic Research Papers 49(12):2163–2181. https://doi.org/10.1016/S0967-0637(02)00122-X

Krembs C, Eicken H, Deming JW (2011) Exopolymer alteration of physical properties of sea ice and implications for ice habitability and biogeochemistry in a warmer Arctic. Proceedings of the National Academy of Sciences 108(9):3653–3658. https://doi.org/10.1073/pnas.1100701108

Lake RA, Lewis EL (1970) Salt rejection by sea ice during growth. Journal of Geophysical Research 75(3):583–597. https://doi.org/10.1029/JC075i003p00583

Lannuzel D, Tedesco L, Van Leeuwe M, et al (2020) The future of Arctic sea-ice biogeochemistry and ice-associated ecosystems. Nature Climate Change 10(11):983–992. https://doi.org/10.1038/s41558-020-00940-4

Miller LA, Fripiat F, Else BG, et al (2015) Methods for biogeochemical studies of sea ice: The state of the art, caveats, and recommendations. Elementa: Science of the Anthropocene 3:000038. https://doi.org/10.12952/journal.elementa.000038

Petrich C, Eicken H (2009) Growth, structure and properties of sea ice. In: Sea Ice. John Wiley & Sons, Ltd, chap 2, p 23–77, https://doi.org/10.1002/9781444317145.ch2

Riedel A, Michel C, Gosselin M (2006) Seasonal study of sea-ice exopolymeric substances on the Mackenzie shelf: Implications for transport of sea-ice bacteria and algae. Aquatic Microbial Ecology 45:195–206. https://doi.org/10.3354/ame045195

Roukaerts A, Deman F, Van Der Linden F, et al (2021) The biogeochemical role of a microbial biofilm in sea ice. Elem Sci Anth 9(1):001–14. https://doi.org/10.1525/elementa.2020.00134

Steffen KR, Epshteyn Y, Zhu J, et al (2018) Network Modeling of Fluid Transport Through Sea Ice with Entrained Exopolymeric Substances. Multiscale Modeling & Simulation 16(1):106–124. https://doi.org/10.1137/17M1117513

Stoecker DK, Gustafson DE, Baier CT, et al (2000) Primary production in the upper sea ice. Aquatic Microbial Ecology 21(3):275–287. https://doi.org/10.3354/ame021275

Tedesco L, Vichi M (2014) Sea ice biogeochemistry: A guide for modellers. PLoS ONE 9(2):e89217. https://doi.org/10.1371/journal.pone.0089217

Thomas DN, Dieckmann GS (2010) Sea Ice, 2nd edn. Wiley-Blackwell, https://doi.org/10.1002/9781444317145

Zong Z (2022) A Random Pore Model of sea ice for predicting its mechanical properties. Cold Regions Science and Technology 195:103473. https://doi.org/10.1016/j.coldregions.2021.103473